IOP Conf. Series: Materials Science and Engineering **382** (2018) 042006 doi:10.1088/1757-899X/382/4/042006

Design and Improvement of the Investment Casting Process for the Ring-shaped Aluminum Alloy based on PROCAST software

Jukui GUO[1*], Yongxin LI[1], Jia FU[2,3*]

[1]Xi'an Brake Branch, AVIC Aircraft Co., LTD., Xinping, 713106, China;

[2]School of Material science and engineering, Xi'an Shiyou University, Xi'an, 710065, China;

[3]Material science and engineering, Taiyuan university of science and technology, taiyuan, 030024, China;

Email: guojukui@163.com; fujia@xsyu.edu.cn

Abstract: The investment casting process of a ring-shaped ZL101 alloy is investigated based on PROCAST software, the alloy phase diagram and the thermophysical properties are analyzed. Besides, the initial casting temperature and the casting process were determined. After the analysis of the geometry model and temperature field model during the casting solidification process, results shows as: 1) the shrinkage and porosity is formed at the two sides and bottom end of casting pieces in the initial casting process, while slag inclusion is enriched at the top. 2) To avoid these two kinds of defects, the casting process is optimized and simulated. The simulated result is in compliance with the experiment, the agreement confirm that the improved process is reasonable. 3) The improved casting process is finally designed and the simulation shows that the experiment is in good agreement with the simulation results, which provides the actual guidence for the design of other casting pieces as well.

1. Introduction

With the development of computer technology, material physical parameters can be calculated through first-principle theory, molecular dynamics and others to provide support for performance calculation[1-4]. For the vast majority of aluminium-based casting alloys, the main second phase has a lots of forms, typically of intricate networked or isolated particles, depending on the alloy composition and processing history [5-9]. Recently, more and more scholars pursuit the light deformation and near net shape deformation, in the aviation industry, spaceflight industry, automobile industry, ship industry, weapons industry, electronic industry and other fields. This also put forward higher request of the complicated, thin-walled and motors casting process [10]. The melting mode method makes aluminum alloy casting have a place in the field of aerospace light parts production [11-12]. In order to reduce cost and energy consumption, casting simulation software is commonly used as an auxiliary tool for the design and improvement of casting process [13]. Based on the shape characteristics of the ring aluminum alloy, preliminary investment casting process is designed, the temperature field, shrinkage distribution, slag inclusion distribution are simulated. The simulated results help to optimize the new casting process, which makes the simulation optimize the casting process and is meaningful to the practical production.

2. Description of material characteristic and mathematical solidification process

2.1. Composition, phase diagram and thermo-physical properties' parameters

The chemical compositions of ZL101 Magnesium alloy were (wt.%): Si: 7.0, Mg: 0.3, Al: (balance). Based on this material's database in PROCAST, some of the thermal physical parameters can be used to calculate the phase diagram, the density curve and thermal conductivity curve with the change of temperature, in Figure 1.

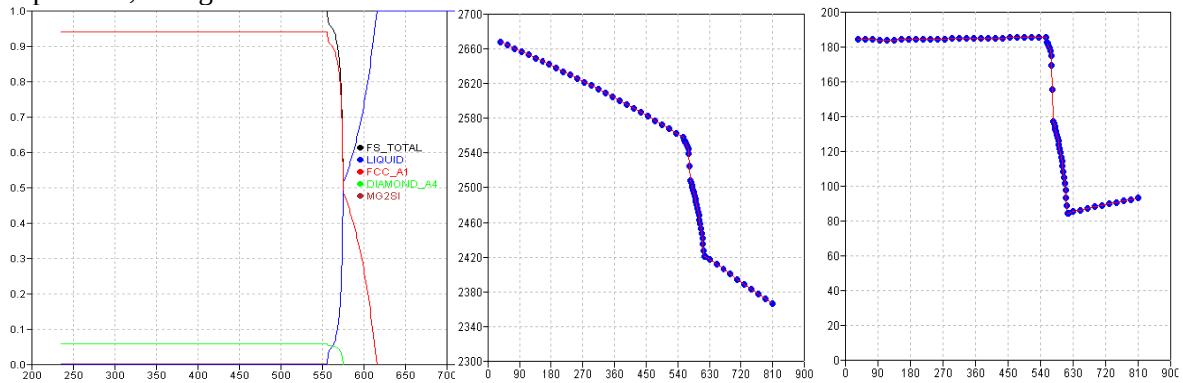

(a) Phase diagram (b) Density (c) Thermal conductivity

Figure 1 Phase diagram, density curve and thermal conductivity curve of ZL101 alloy

As is seen in the right sign of Figure 1 (a), the alloy phase diagram of ZL101 (subtotal Al-Si) mainly includes the α-Al zone (the FCC-A1), the homogeneous Si phase (DIAMOND_A4, the particle form) and the liquid phase region, and a very small amount of Mg_2Si. Within the range of lower than 556℃, the alpha Al phase in the ZL101 mainly existed, also with about 7% of the granular Si and very little Mg_2Si. For the region from the initial liquid temperature (556℃) to the eutectic temperature (577℃), the alpha phase Al is coexisted with elemental Si phase and the liquid form. Between 577℃ and 616℃, the primary alpha-Al is gradually precipitated in the liquid. Pouring temperature should be selected higher than the liquid zone (556-616℃) about 70-110℃. The density curve and thermal conductivity curve versus temperature are in Figure 1 (b) and (c).

2.2 Description of the mathematical model during solidification process

The mathematical model of heat transfer by using Fourier thermal differential equation [14] is as:

$$\rho c_p \frac{\partial T}{\partial t} = \frac{\partial}{\partial x}\left(\lambda \frac{\partial T}{\partial x}\right) + \frac{\partial}{\partial y}\left(\lambda \frac{\partial T}{\partial y}\right) + \frac{\partial}{\partial z}\left(\lambda \frac{\partial T}{\partial z}\right) + \dot{Q} \tag{1}$$

Where, c_p is the quality specific heat capacity, λ is thermal conductivity, T is the temperature, t is time, $\dot{Q}$ is the internal heat source, ρ is the density, x、y、z are the three-dimensional coordinates.

The equivalent heat capacity method [15] is used to deal with the crystallization latent heat, thus:

$$\dot{Q} = \rho Q \frac{\partial f_s}{\partial t} = \rho Q \frac{\partial f_s}{\partial T} \bullet \frac{\partial T}{\partial t} \tag{2}$$

Where, f_s is the solid phase ratio at the temperature T, $\dot{Q}$ is the crystallization latent heat of the alloy, which is a function of temperature.

It is assumed that the crystallization latent heat in the solidified interval is released uniformly, thus the solid phase ratio and temperature turns to be a linear relationship, which is as [16]:

$$f_s = \frac{T_1 - T}{T_1 - T_s} \tag{3}$$

Where T_l is the temperature of the liquid phase line; T_s is the temperature of the solid phase line.

The initial conditions and boundary conditions [16] are as follows:

$$T(x,y,z,t)\big|_{t=0} = T_0 \tag{4}$$

$$-\lambda \frac{\partial T}{\partial n}\big|_s = h(T_1 - T_2) \tag{5}$$

Where, h is interfacial heat transfer coefficient between piece and mold; T_0 is the initial temperature, T_1 is the piece interfacial contact temperature; T_2 is the mold interface temperature.

3. Casting piece's design and the FEM model

The ring-shaped alloy are formed by melting mould casting process, the model of ring piece and casting system is shown in Figure 2.

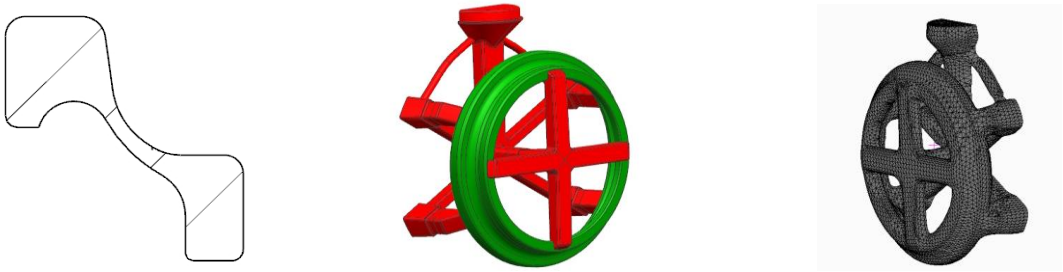

(a) Ring section (b) Geometry model of casting system (c) Grid model of casting system
Figure 2 The model of ring piece and casting system

As shown in Figure 2, the section shape of the ring part is in Figure 2 (a). The 3D models of casting and pouring system are done in CATIA software, in Figure 2 (b). The model in Figure 2 b) was then imported into PROCAST, with a total grid of 79823, with a total unit of 336,677, in Figure 2 c). In the PROCAST module, the materials model, interface conditions, boundary conditions, other initial conditions and operation parameters are set up in PROCAST for simulate the casting processes.

4. Simulation analysis and discussion

The maximum peripheral dimensions of the castings are 500*mm*×500*mm*×35*mm*, and the minimum wall thickness is 3*mm*, so four pouring gates are added and staggered on both left and right sides. Due to the characteristic of high thermal conductivity, high heat transfer of shell mould, and a minimum wall thickness of 3*mm* in ZL101 alloy, the pouring temperature for simulation is chosen 710℃ considering all practical situation.

4.1 Analysis of the temperature field and prediction of shrinkage and slag inclusion

To study the solidification temperature field and defects after the optimization of casting process, the Niyana criterion [17] embedded in PROCAST software is used to accurately predict the shrinkage of various parts of the ZL101 casting, shown in Figure 3.

a b

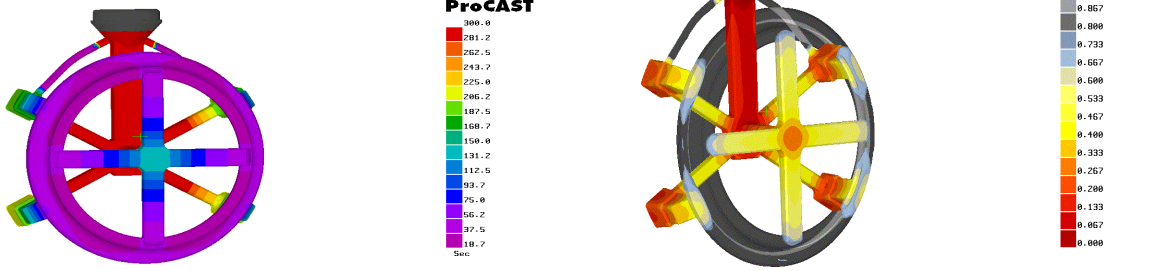

(a) the solidification temperature versus time (b) the solidification sequence distribution

c d

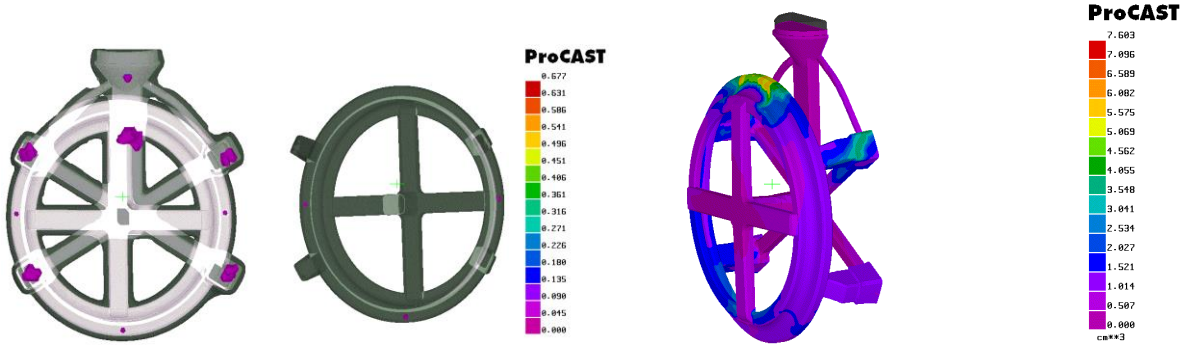

(c) the shrinkage distribution (d) the slag inclusion distribution

Figure 3 The solidification temperature field and defects after the optimization of casting process

The change of temperature in the ring parts with the increase of the solidification time is shown in Figure 3 (a). It is found that the solidification is basically finished using 56s, and the central cross pouring gate is overlapped in the feeding areas of sprue gate, which may forms the "feeding disorders [18]," or even forms " feeding gasp" phenomenon, thus leads to the formation of shrinkage. The time cloud map in the solidification process was analyzed in Figure 3 (b), the solidification sequence analysis of casting process shows the apparent liquid phase isolation in three parts of the ring piece, which fatherly proves the possible appearance of shrinkag.

As is shown in Figure 3 (c), the simulation of the shrinkage distribution shows a small amount of shrinkage on both sides and lower ends of ring piece. According to the algorithm of the "metal flow frontier ion tracking" in PROCAST and the observation of the flow convergence situation [19], the simulation in Figure 3 (d) shows the most of slag inclusion is clustered at the top end of the ring piece.

4.2 Improvement of the initial casting process

Although the casting achieves the purpose of sequence solidification, the shrinkage area of the casting is reduced due to the long channel of the metal liquid and the temperature reduced rapidly in the center, thus leads to shrinkage defect. Besides, the casting system is not good enough to drainage the slag inclusion, and it is easy to form the slag inclusion in the casting, especially the high density slag inclusion, which has a serious impact on the product quality and performance. So we can infer that the initial process is not good and acceptable.

For the shrinkage problem, the gate at the bottom is added to eliminate the shrinkage problem at the lower end. In the case of the shrinkage on the left and right sides, the heat preservation of the pouring gate is done, which makes the two sides of the "shrinkage disturbance" zone form a large temperature gradient, thus eliminating the shrinkage between the casting channel and casting gate.

In view of these two kinds of defects, we have made improvement of casting process. Defects of shrinkage and slag inclusion after the optimization of the casting process are shown in Figure 4.

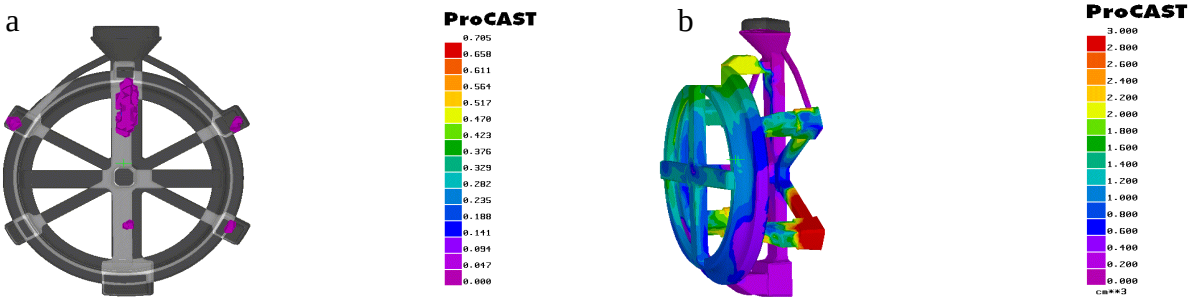

(a) Shrinkage distribution (b) Slag inclusion distribution

Figure 4 Defects of shrinkage and slag inclusion after the optimization of the casting process

The modified casting scheme is simulated and the shrinkage problem is avoided in Figure 4 (a). Meanwhile, it is also found in Figure 4 (b) that the slag inclusion easily enriched in the casting has been solved. The improved process can not only eliminate the shrinkage but also enhance the stability of the process, reducing the risk of shrinkage due to the process fluctuation in the production.

For the problem of slag inclusion, the gating system has been optimized and the similar dark casting gate is added at the upper part, which let the slag inclusion fluent as much as possible through the gate to collect the slag inclusion on the top during the filling process. Moreover, the added gate also plays a role of balancing the filling speed and slag inclusion during the castings and has certain feeding effect at the same time.

4.3 Verification of the experimental casting process

From the above analysis, the shrinkage prediction results are consistent with results of the temperature field analysis. The improved process based on the simulation optimization is validated by the casting process tests, by two kinds of simulation process. According to the slag inclusion position under two processes, samples are done in the same place to compare its slag inclusion and microstructure morphology validation, in Figure 5.

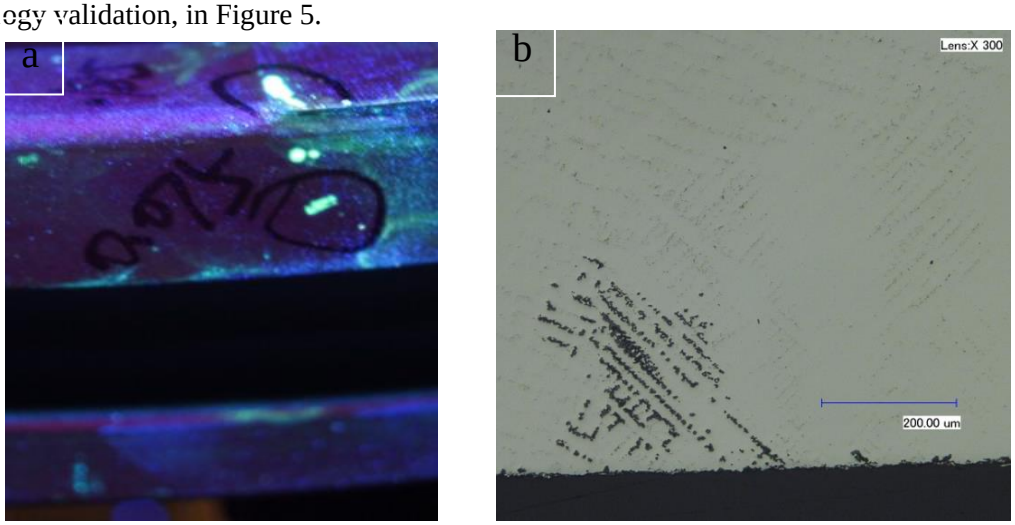

(a) Slag inclusion distribution in FPI (b) Metallography image of the corresponding slag inclusion

Figure 5 Slag inclusion, shrinkage and porosity in FPI by metallography image

As shown in Figure 5 (a), the fluorescence detection shows the overweight of two slag inclusion areas appeared in direction of the upper of tree under the initial process, consistent with the slag inclusion simulated location. While under the improved process there is no the slag inclusion area caused by overweight. On the other hand, the position of the shrinkage was predicted in the initial process simulation. The X-ray detection is done at the position, then the samples is cut and metallographic analysis of its position is agree with the simulation expectation, shown in Figure 5 (b). Overall, through the experimental verification of the improved process, it is found that the results of the experiment and simulation are completely consistent. This agreement suggests that defects are effectively predicted based on the analysis by PROCAST, which has guided the practical production and met the requirement of quality and size.

5. Conclusions

The investment casting process of ZL101 ring-shaped alloy is analyzed and improved based on PROCAST software. Based on the material data inserted in PROCAST, the reasonable actual casting temperature is obtained and the preliminary casting system is designed according to the material intrinsic properties and ring shape. Through the analysis of the simulation, the temperature field, shrinkage and slag inclusion during casting process are discussed. Results are as follows:

(1) The phase diagram of ZL101 alloy is studied through PROCAST where the liquid zone is

556℃ to 616℃ and the initial casting temperature is determined to be 710℃. As the characteristic of thin area in center and thick area along the sides of the casting section, four sprue gates were added on both sides of the thick area.

(2) Based on the simulation analysis of the casting solidification process (solidification time map, shrinkage prediction map, solidification sequence diagram), the shrinkage was forecast to be likely appeared on both sides and the bottom position of the piece, while the slag inclusion is easily enriched in the upper position.

(3) Based on the simulation and prediction results, the casting system and heat preservation are optimized and improved, and the problems of shrinkage and slag inclusion are both avoided.

(4) The experiment by the modified process scheme was carried out and the simulation result, which is thought to be quite consistent with experiment, thus verified the reliability of the simulation results.

Acknowledgements
The authors greatly acknowledge the financial support for this work provided by Natural Science Foundation of China (No.51174140), and the support of the Xi'an Brake Branch in AVIC Aircraft Co., LTD..

References

[1] Jia Fu, B. Fabrice, K.B. Siham, Assessment of the elastic properties of amorphous Calcium Silicates Hydrates (I) and (II) structures by Molecular Dynamics Simulation[J]. Molecular Simulation.2017, 44(05):1-15.
[2] Jia Fu, B. Fabrice, K.B. Siham. First-principles calculations of typical anisotropic cubic and hexagonal structures and homogenized moduli estimation based on the Y-parameter[J]. Journal of Physics and Chemistry of Solids,2017,101: 74-89.
[3] Jia Fu, B. Fabrice, K.B. Siham, Multiscale Modeling and Mechanical Properties of Zigzag CNT and Triple-Layer Graphene Sheet Based on Atomic Finite Element Method[J]. J. Nano Research. 2015, 33:92-105
[4] Jia Fu, Yongtang Li, Huiping Qi. Microstructure simulation and experimental research of as-cast 42CrMo steel during quenching process, Advanced Materials Research, 317-319 (2011):19-23.
[5] R. Doglione, In situ investigations on the ductility of an Al-Si-Mg casting alloy[J]. JOM, 2012, 64: 51-57.
[6] H. Toda, P. Qu, S. Ito, K. Shimizu, K. Uesugi, A. Takeuchi, Y. Suzuki, M. Kobayashi, Formation behaviour of blister in cast aluminium alloy[J]. Int. J.Cast. Metal. Res.,2014, 27:369-377.
[7] I. Gattelli, G. Chiarmetta, M. Boschini, R. Moschini, M. Rosso, I. Peter, New generation of brake calipers to improve competitiveness and energy saving in very high performance cars[J]. Solid State Phenom.,2015, 217: 471-480.
[8] S. Janudom, J. Wannasin, J. Basem, S. Wisutmethangoon, Characterization of flow behavior of semi-solid slurries containing low solid fractions in high-pressure die casting[J]. Acta Mater.,2013, 61: 6267-6275.
[9] S.P. Midson, Industrial applications for aluminum semi-solid castings[J]. Solid State Phenom. 2014, 217: 487-495.
[10] Sajjadi S A, Ezatpour H R, Parizi M T. Comparison of microstructure and mechanical properties of A356 aluminum alloy/Al_2O_3 composites fabricated by stir and compo-casting processes[J]. Materials & Design, 2012, 34: 106-111.
[11] Lu S, Xiao F, Guo Z, et al. Numerical simulation of multilayered multiple metal cast rolls in compound casting process[J]. Applied Thermal Engineering, 2016, 93: 518-528.
[12] Pattnaik S, Karunakar D B, Jha P K. Developments in investment casting process—a review[J]. Journal of Materials Processing Technology, 2012, 212(11): 2332-2348.
[13] SAROJRANI P,BENNY K D , JHAPK. Developments in investment casting process-A review [J]

Journal of materials Processing Tech- nology , 2012,212:2332-2348.
[14] Fu J, Wang K. Modelling and simulation of die casting process for A356 semi-solid alloy[J]. Procedia Engineering, 2014, 81: 1565-1570.
[15] Jukui Guo, Jianli Song, Jia Fu, et al. Simulation of temperature field of modified medium manganese steel liner by inclined casting based on ProCAST [J] Special Casting & Nonferrous Alloys, 2014, 34(10): 1050-1053.(in Chinese)
[16] Brůna M, Bolibruchová D, Pastirčák R. Numerical Simulation of Porosity for Al Based Alloys[J]. Procedia Engineering, 2017, 177: 488-495.
[17] Rappaz M. Modeling of microstructure format-ion in solidification Processes [J].International Materials Reviews, 1989, 34(1): 93-12
[18] Dong Y W, Li X L, Zhao Q, et al. Modeling of shrinkage during investment casting of thin-walled hollow turbine blades[J]. Journal of Materials Processing Technology, 2017, 244: 190-203.
[19] Lu S L, Xiao F R, Zhang S J, et al. Simulation study on the centrifugal casting wet-type cylinder liner based on ProCAST[J]. Applied Thermal Engineering, 2014, 73(1): 512-521.